Appl. Math. Mech. -Engl. Ed., **43**(3), 437–446 (2022)

APPLIED MATHEMATICS AND MECHANICS (ENGLISH EDITION)

https://doi.org/10.1007/s10483-022-2820-5

Droplet impact on wetted structured surfaces*

M. MOHASAN[1], A. B. AQEEL[1,2], Huiling DUAN[1,3], Pengyu LYU[1], Yantao YANG[1,†]

1. Department of Mechanics and Engineering Science, State Key Laboratory for Turbulence and Complex Systems (SKLTCS), Beijing Innovation Center for Engineering Science and Advanced Technology (BIC-ESAT), College of Engineering, Peking University, Beijing 100871, China;
2. Department of Mechatronics Engineering, National University of Sciences and Technology, Islamabad 44000, Pakistan;
3. Center for Applied Physics and Technology (CAPT), HEDPS and IFSA Collaborative Innovation Center of MoE, Peking University, Beijing 100871, China

(Received Aug. 8, 2021 / Revised Dec. 13, 2021)

Abstract In this study, we numerically investigate the droplet impact onto a thin liquid film deposited on a structured surface with square pillars and cavities. The time evolution of crown geometry is strongly affected by the surface structure. When the thickness of the liquid film is larger than the structure height, the expanding speed of the crown base radius is independent of the structure width. However, if the liquid film thickness is equal to the structure height, the crown base expands slower as the structure width increases. Surface structures have strong effects on the crown height and radius, and can prevent ejected filament from breaking into satellite droplets for certain cases. For the liquid film with the thickness equal to the pillar height, both the crown height and the radius exhibit non-monotonic behaviors as the pillar width increases. There exists one pillar width which produces the smallest crown height and the largest crown radius.

Key words droplet impact, structured surface, liquid film, crown formation

Chinese Library Classification O363.2
2010 Mathematics Subject Classification 76D45

1 Introduction

Droplet impact on surface of liquid or solid has been an active topic for a very long time. Phenomena of the droplet impact on surface wetted with liquid film are available in nature and in many applications of industrial products, such as inkjet printing[1], spray cooling and painting[2], internal combustion engines[3], and agricultural applications[4–5]. Such a process

* Citation: MOHASAN, M., AQEEL, A. B., DUAN, H. L., LYU, P. Y., and YANG, Y. T. Droplet impact on wetted structured surfaces. *Applied Mathematics and Mechanics* (*English Edition*), **43**(3), 437–446 (2022) https://doi.org/10.1007/s10483-022-2820-5

† Corresponding author, E-mail: yantao.yang@pku.edu.cn

Project supported by the National Natural Science Foundation of China (Nos. 11988102, 91848201, 11872004, and 11802004)

induces very rich dynamical phenomena, including droplet rebound, splashing, fusion with film, and crown structures of different shapes[6–7]. It has been shown that the crown structures and splashing behaviors are strongly influenced by the velocity of the impacting droplet, properties of the droplet fluid, and thickness of the liquid film[8–10].

The structural geometry and properties of surface also strongly influence the impact dynamics[11–13]. For example, when the droplet impacts on a lotus leaf which contains micro-size structures on its surface, it will generate splash or secondary drops on the lotus leaf[14–15]. With droplet impact on dry solid surface, it spreads to produce a shape of lamella which can deposit completely, and bounce back from the surface, or may result in splashing due to the influence of physical parameters[16–17]. Lee et al.[18] determined the maximum value of the droplet spreading after impacting on the surface with micro-structures and revealed that the wettability property of the micro-structure surface influences the outcome dynamics of impacting liquid droplets. Kannan and Sivakumar[19] analyzed the impact of droplet phenomena on the surface of micro-cavities. They reported that the behavior of spreading liquid is influenced by the cavity structure. Lakta et al.[20] identified that splashing is produced when a viscous droplet impacts on the rough surface. Xu[21] found that surface morphology was an important factor for droplet impact to produce prompt splash on these solid surfaces.

Meanwhile, a lot of numerical and experimental investigations have been reported in the literature for droplet impact on liquid films with multiple conditions[6,8], focusing on the splash mechanism[22], the horizontal and vertical growth of crown[10], and the height of the Worthington jet[23–25]. Cossali et al.[26] analyzed the crown shape formation with the droplet impact on an aluminium disc wetted with a very thin layer of water or water-glycerol liquid. Rioboo et al.[22] addressed the crown formation generated by the droplet impact onto the liquid film of very small thickness with a very high impact velocity. Influence of film thicknesses, liquid properties, and operating conditions has also been systematically studied by several groups, such as Lee et al.[27] and Mukherjee and Abraham[28].

The above discussions suggest that both surface structure and liquid film thickness can strongly affect the droplet impact dynamics. In the current study, we combine the two factors and investigate the drop impact on a thin liquid film deposited on a solid structured surface. We perform numerical simulations for the impact of water droplets on the surface containing sequence of rectangular pillars of fixed height and different widths wetted with liquid film of different thicknesses. Based on the results of explored simulations, we concentrate on the crown evolution on the impacted surface including crown jet height and crown radius.

The paper is arranged as follows. Section 2 describes the computational flow domain, the numerical technique, and its validation. Section 3 contains the main results and discussions. Finally, Section 4 contains the conclusions of this work.

2 Flow setup and numerical methods

We consider a two-dimensional model as shown in Fig. 1. A liquid film with height h is located over the bottom boundary of the domain which has alternately distributed square pillars and cavities. The film thickness is measured from the top surface of the pillars to the upper region of the liquid film. The vertical height of the pillars (or the cavity depth) is fixed at $h_s = 100\,\mu m$. The pillars and cavities always have the same width w_s, which will be changed systematically in our simulations. A drop with fixed diameter $D = 1\,mm$ is placed initially just above the top surface of the film, with the drop center on top of the center of one pillar. The liquid is the same as the drop and film, and the fluid is set as air outside the liquid phase. Two key nondimensional parameters are the Reynolds number and the Weber number defined as $Re = \rho DU/\mu$ and $We = \rho DU^2/\sigma$, respectively. Here, ρ represents the liquid density, the impacting velocity is denoted by U, and the dynamic liquid viscosity and surface tension are represented by μ and σ, respectively.

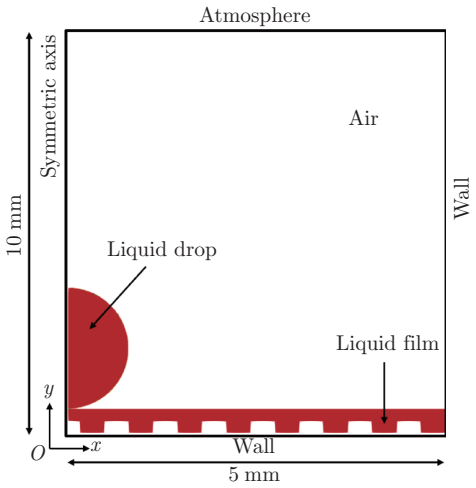

Fig. 1 Geometry and initial phase representation of the numerical simulations (color online)

We assume that the flow is symmetric about the vertical line through the drop center, and therefore, only half of the domain is simulated. The half domain has a width of 5 mm and a height of 10 mm. The bottom structured boundary is no-slip, while the upper boundary is open atmosphere with a far-field condition. The left vertical wall is symmetric, and the right one is no-slip. We denote the horizontal axis as x and the vertical one as y, respectively. An open-source solver of OpenFoam, which is known as InterFOAM, is utilized to simulate the incompressible flow. The standard volume of fluid (VoF) method is considered for the multiphase part, i.e., for the volume fraction of each phase an extra equation is solved. For the computation of surface tension force, the continuum surface force model is utilized[29]. In order to capture a sharp interface, an additional convective term is included in the equations for the volume fractions, as done by Weller[30]. The pressure-velocity coupling is dealt with the PISO technique.

To validate our numerical method, we simulate the impact of a droplet onto a flat surface covered with liquid film and compare our results with the simulations of Shetabivash et al.[31] and the experimental outcomes of Cossali et al.[10]. The control parameters are chosen as the same, which are $h/D = 0.29$, $Re = 13\,676$, and $We = 667$, respectively. The comparison for the temporal history of the crown radius growth is shown in Fig. 2. Our numerical results are very close to that given by the numerical computations of Shetabivash et al.[31]. Both simulations

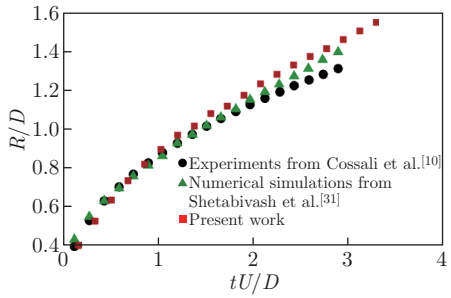

Fig. 2 Comparison among the experimental outcomes from Cossali et al.[10], the numerical outcomes from Shetabivash et al.[31], and our numerical simulation results for the time history of the crown radius ($We = 667$, and $h/D = 0.29$) (color online)

agree reasonably with the experimental plots of Cossali et al.[10], especially during the initial growth of crown. At the later stage, the crown radii given by the two numerical studies are both slightly higher than that of experiments.

Especially for the structured boundary in the present study, extra test simulations are carried out to further validate the numerical settings. Larger domain width has been tested, and no significant changes are observed in the impacting dynamics, indicating that the current width is large enough. Besides, the effect of the initial gap between the drop and the film is evaluated. In the current simulations, the drop is located right above the top surface of film initially. In the real physical process of drop impact on the surface of a liquid pool, the liquid surface may deform before the drop touches the liquid, which may affect the dynamics of the impacting. To illustrate that our initial configuration is not influenced by such a phenomenon, we run a group of cases with different initial gaps between the drop and the liquid film, namely, $0D$, $0.02D$, and $0.05D$. For these three simulation cases, the phase distributions at 1.1 ms after the impact are shown in Fig. 3. The fluid flow fields are almost identical to each other. There are some visible differences at the top part of the filament, especially near the neck of the tip droplet. This is mainly due to the fact that the air flow and pressure distribution inside the gap between the droplet and the film surface are different for different initial gaps. For thick liquid films or deep pools, the surface can have large deformation right before the droplet touches the surface, and the initial gap has larger effects on the crown dynamics. For the relatively thin film used here, the deformation of the surface before impact is small due to the confinement from the bottom boundary, and therefore, only minor changes appear for different cases in Fig. 3.

Since we mainly concentrate on the effects of the structures and the thickness of the liquid film, the drop velocity is fixed at $U = 3\,\mathrm{m/s}$. Thus, the Reynolds and Weber numbers are fixed correspondingly at $Re = 3\,000$ and $We = 125$. Three different values are considered for the film thickness, i.e., $h = 100\,\mu\mathrm{m}$, $150\,\mu\mathrm{m}$, and $200\,\mu\mathrm{m}$. The pillar and cavity width are increased systematically from $50\,\mu\mathrm{m}$ to $600\,\mu\mathrm{m}$. The explored parameters are shown in Fig. 4. For the lower part of the domain where the impacting occurs, uniform meshes with a cell size $2\,\mu\mathrm{m}$ are used to capture the key flow phenomena. Thus, for the smallest cavity width $w_\mathrm{s} = 50\,\mu\mathrm{m}$, there are 25 meshes distributed horizontally and 50 meshes distributed vertically, respectively. For the upper part, meshes are stretched in the vertical direction with increasing cell size to save the computing cost. The lower region with uniform mesh has a height of 2 mm. Finer meshes are tested, and quantitative agreement is obtained.

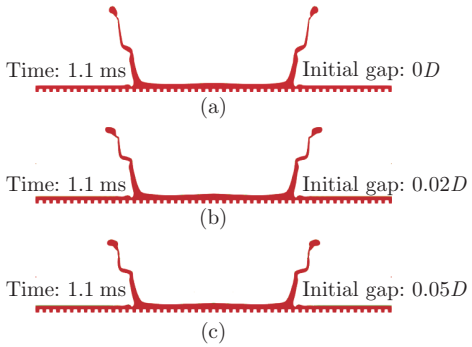

Fig. 3 Crown shapes at the same time after drop impacting for different initial gaps between the drop and film surface: (a) $0D$; (b) $0.02D$; (c) $0.05D$ (color online)

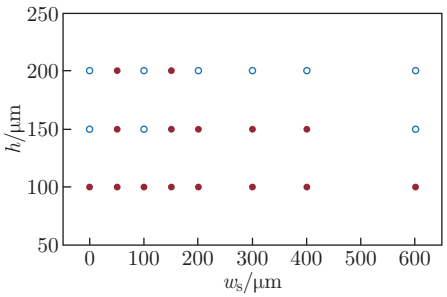

Fig. 4 Explored pillar width and film thickness in the current study (open blue circles mark the cases with jet breakup, while solid red ones are without jet breakup, respectively) (color online)

3 Results and discussion

3.1 Two types of crown evolution

After impacting onto the liquid film, the drop deforms and stretches horizontally. Filaments are ejected from the edge to develop a crown geometry. The height and radius of the crown grow with time. Two types of crown evolutions can be identified based on the later fate of the ejected filament, which are shown in Fig. 5. For some cases, the filament remains connected during the entire simulation, while for others, the tip of filament breaks and generates small droplets. We mark the two types of cases in the parameter space shown in Fig. 4.

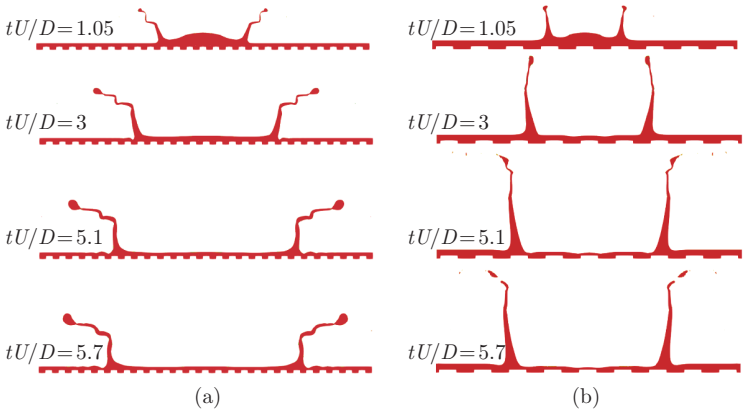

Fig. 5 Two types of crown evolution: (a) no filament breakup for $h = 100\,\mu\text{m}$ and $w_s = 200\,\mu\text{m}$; (b) filament breakup for $h = 200\,\mu\text{m}$ and $w_s = 600\,\mu\text{m}$ (color online)

For the film thickness $h = 100\,\mu\text{m}$, the filament does not break for the plain surface, and for all the pillar widths considered here. For two larger film thicknesses, breakup happens for the plain surface without structures. Surface structures can prevent this breakup of filament at certain pillar widths. As the film thickness h increases, the range of the pillar width within which the breakup is eliminated shrinks. Interestingly, the smallest pillar width of $w_s = 50\,\mu\text{m}$ can prevent breakup for both $h = 150\,\mu\text{m}$ and $h = 200\,\mu\text{m}$, while pillars with $w_s = 100\,\mu\text{m}$ do not. A complete phase diagram for the breakup/non-breakup regimes requires further simulations over a wider parameter range.

3.2 Effects of the pillar width

In this section, we focus on the cases with the film thickness $h = 100\,\mu\text{m}$. For these cases, the crown filaments do not break. To quantitatively measure the evolution of the crown, we determine the time histories of three characteristic lengths, as shown in Fig. 6. The radius R_b of the crown base is measured at the height which is twice the thickness of the liquid film for all cases. When the crown filament does not break up, we also measure both the radial location R and the height H of the filament tip.

In Figs. 7 and 8, we plot H, R, and R_b versus time for all cases. Both R and H exhibit complex behaviors as the pillar width increases. H reaches a saturated value when $tU/D > 6$. We calculate the averaged H over the time period $tU/D > 6$. The dependence of this averaged height $\overline{H}$ on the pillar width w_s is displayed in Fig. 7(b). Clearly, $\overline{H}$ exhibits a non-monotonic variation. As the pillar width increases from 0, it increases rapidly. Then for $w_s = 200\,\mu\text{m}$ and $300\,\mu\text{m}$, it reduces to a value smaller than that for the plain boundary situation. As w_s becomes even larger, $\overline{H}$ increases again. One can anticipate that as w_s becomes much larger than the drop diameter D, the flow will be the same as the plain surface. For the set of cases discussed here, the pillar widths of $w_s = 200\,\mu\text{m}$ and $300\,\mu\text{m}$ generate the smallest jet height $\overline{H}$ during

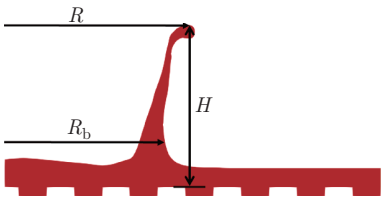

Fig. 6 Definitions of the crown base radius R_b, the radial location R, and the height H of the filament tip (color online)

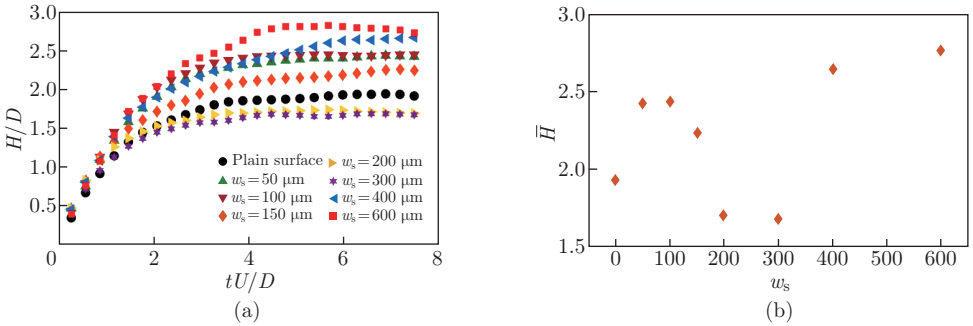

Fig. 7 For the fixed film thickness $h = 100\,\mu$m, (a) the effects of the pillar width on the crown jet tip height H and (b) the saturated crown height $\overline{H}$ at the final stage versus the pillar width (color online)

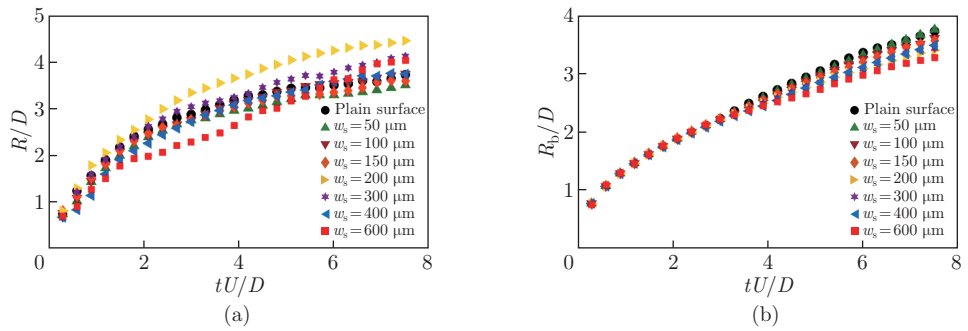

Fig. 8 Effects of the pillar width on the crown geometry for the fixed film thickness $h = 100\,\mu$m with (a) the radial location R of tip and (b) the radius R_b of the crown base (color online)

the saturated stage.

The change of the pillar width has more complex effects on the radial movement of the crown tip, as shown in Fig. 8(a). After $tU/D > 2$, the curves are very scattered for different w_s. R is the largest for the pillar width $w_s = 200\,\mu$m. Recall that for this width, the crown height is the smallest. Then, for this case, the crown develops mainly horizontally. Figure 8(b) displays the variations of the crown-base radius R_b for different pillar widths. For all cases, R_b increases almost identically until $tU/D \approx 3$. As w_s becomes larger, R_b is smaller. Therefore, a large pillar width imposes higher resistance from below, and reduces the expanding speed of the crown-base at the later stage.

The evolutions of the flow field are shown for five cases with different pillar widths in Fig. 9.

The cases of $w_s = 200\,\mu m$ and $w_s = 300\,\mu m$ are shown in columns (c) and (d), which have the smallest $\overline{H}$ and the largest R among all the pillar widths for $h = 100\,\mu m$. The evolutions of the lower part of filaments are very similar among cases with different pillar widths. But the upper part of the filaments has very different behaviors for different cases, which generate different crown heights and radii at the tip. Moreover, the filament shape at the later stage is totally determined by its early shape. Specifically, in the top row of Fig. 9, the filaments of all cases bend inwards, except for the cases with $w_s = 200\,\mu m$ and $w_s = 300\,\mu m$, which have the crown tip pointing outwards. This difference maintains the entire development of the crown, and causes the crown of cases $w_s = 200\,\mu m$ and $w_s = 300\,\mu m$ which have the smallest height and the largest tip radius at the final stage.

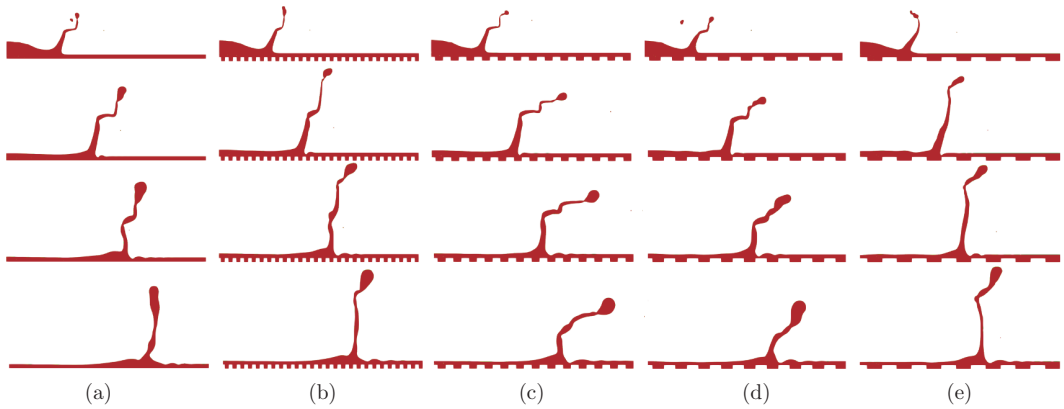

Fig. 9 Crown evolution for five cases with the film thickness $h = 100\,\mu m$. Panels (a)–(e) are for the plain surface and $w_s = 100\,\mu m$, $200\,\mu m$, $300\,\mu m$, and $400\,\mu m$, respectively. Rows from top to bottom correspond to $tU/D = 1.05$, 3, 5.1, and 7.05, respectively (color online)

Another interesting observation from Fig. 9 is that filaments have various bending with different numbers and directions for different pillar widths. This is caused by the interaction between the liquid film and the boundary structures during the spreading of the droplets. It is very likely that as liquid moves outward, vortices can be generated from the edges of the pillars which may in turn generate bending in the growing filament. More detailed investigations into this issue will be of great interest and require more simulations in future.

3.3 Effects of the film thickness

We now look at the effects of the film thickness. In Fig. 10, we show the variations of R_b for the cases with $h = 150\,\mu m$ and $h = 200\,\mu m$. Unlike the situation for the film thickness $h = 100\,\mu m$ as shown in Fig. 8(b), the effects of increasing the pillar width weaken significantly for thicker liquid film. With the largest film thickness $h = 200\,\mu m$, R_b follows the same curve for all cases with different w_s. However, for the thinnest film with $h = 100\,\mu m$, the spreading of crown base is affected by the pillar width, especially at the later stage. For $tU/D > 4$, R_b decreases as w_s becomes larger. Note that at the final time, R_b is larger for the smallest film thickness $h = 100\,\mu m$ compared with the other two film thicknesses.

As shown in Fig. 4, for two pillar widths $50\,\mu m$ and $150\,\mu m$, the crown does not break up for all three film thicknesses considered here. To reveal the effects of the film thickness on the crown evolution, we plot the time histories of H and R for these two pillar widths and different film thicknesses in Fig. 11. Initially, for $tU/D \leqslant 2$, the thickness of liquid films only has minor effects on the variations of H and R. After that, H increases to a higher value for a larger film thickness until the end of simulations. Interestingly, the film thickness only has strong effects on R over the time period $2 < tU/D < 6$. At the final stage $tU/D > 6$, R follows almost the

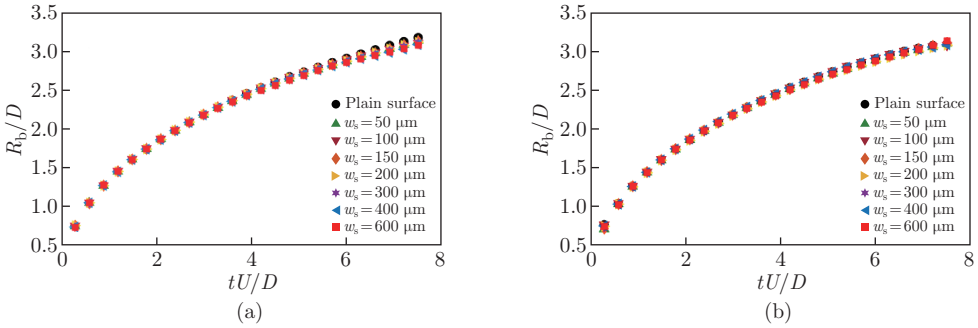

Fig. 10 Time histories of R_b for two larger film thicknesses: (a) $h = 150\,\mu m$; (b) $h = 200\,\mu m$ (color online)

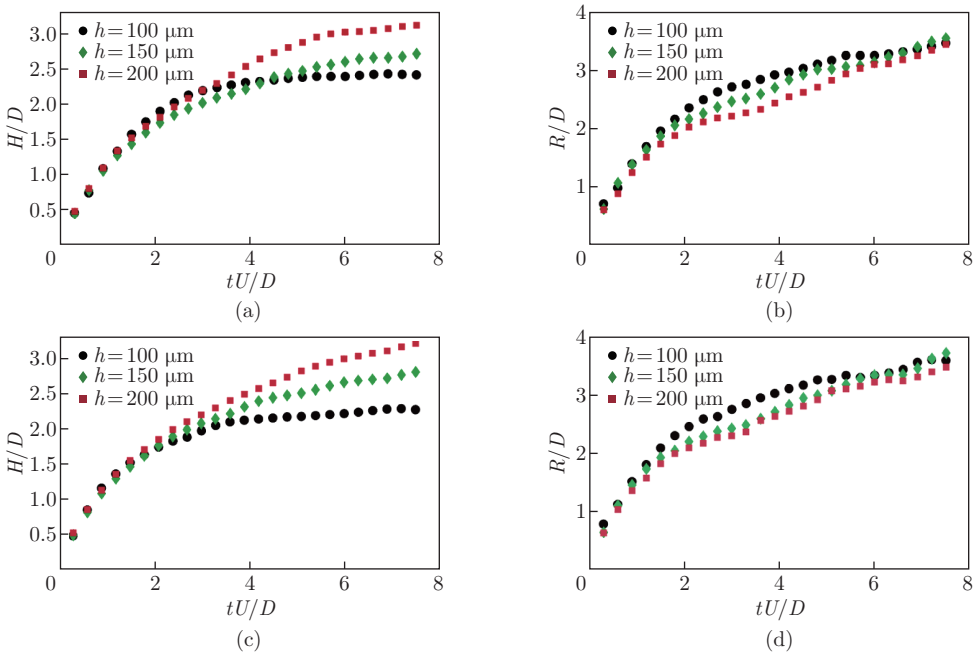

Fig. 11 Trajectories of the filament tip for two fixed pillar widths and different film thicknesses: (a) and (b) top row, $w_s = 50\,\mu m$; (c) and (d) bottom row, $w_s = 150\,\mu m$ (color online)

same evolution for different film thicknesses.

4 Conclusions

In conclusion, we show that for drop impact onto a liquid film of thin size, introducing structures on the surface beneath the liquid film can strongly affect the impact dynamics as long as the structure height is comparable to the liquid film thickness. Current results reveal that when the thickness of the liquid film is twice the structure height, the expansion of the crown base is hardly influenced by the structure width. However, the dynamics of crown filament can be altered by the surface structure for all three liquid-film thicknesses considered here. For certain structure width, the filament does not break into satellite droplets, although it does break for the plain surface case.

The evolution of crown geometry exhibits very complex dependence on the structure width, especially when the thickness of the liquid film is the same as the structure height. The crown height and radius both vary non-monotonically as the structure width increases. There exists a structure width with which the crown has the smallest height and the largest radius among all the structure widths considered. Detailed investigations of the flow fields reveal that the crown height and radius are strongly affected by the filament shape during the initial time right after the impact. The current study is applicable in internal combustion machines, inkjet printing, and spray-painting equipment. Another important factor is the droplet size. It may have influence on the crown evolution with impact on wetted structured surfaces, which requires further investigations. Similar to the droplet size factor, the present setup involves many control parameters which have not been explored here and are of great interests for future studies.

Acknowledgements The numerical simulations were performed on Tianhe-1A, the National Super Computing Center in Tianjin, China. M. MOHASAN would like to thank Chinese Scholarship Council for providing Chinese Government Scholarship.

References

[1] VAN DER BOS, A., VAN DER MEULEN, M. J., DRIESSEN, T., VAN DEN BERG, M., REINTEN, H., WIJSHOFF, H., VERSLUIS, M., and LOHSE, D. Velocity profile inside piezoacoustic inkjet droplets in flight: comparison between experiment and numerical simulation. *Physical Review Applied*, **1**(1), 014004 (2014)

[2] AZIZ, S. D. and CHANDRA, S. Impact, recoil and splashing of molten metal droplets. *International Journal of Heat and Mass Transfer*, **43**(16), 2841–2857 (2000)

[3] MOREIRA, A., MOITA, A., and PANAO, M. Advances and challenges in explaining fuel spray impingement: how much of single droplet impact research is useful? *Progress in Energy and Combustion Science*, **36**(5), 554–580 (2010)

[4] GILET, T. and BOUROUIBA, L. Fluid fragmentation shapes rain-induced foliar disease transmission. *Journal of the Royal Society Interface*, **12**(104), 20141092 (2015)

[5] GART, S., MATES, J. E., MEGARIDIS, C. M., and JUNG, S. Droplet impacting a cantilever: a leaf-raindrop system. *Physical Review Applied*, **3**(4), 044109 (2015)

[6] REIN, M. Phenomena of liquid drop impact on solid and liquid surfaces. *Fluid Dynamics Research*, **12**(2), 61–93 (1993)

[7] HUANG, Q. and ZHANG, H. A study of different fluid droplets impacting on a liquid film. *Petroleum Science*, **5**(1), 62–66 (2008)

[8] YARIN, A. L. and WEISS, D. A. Impact of drops on solid surfaces: self-similar capillary waves, and splashing as a new type of kinematic discontinuity. *Journal of Fluid Mechanics*, **283**, 141–173 (1995)

[9] WANG, A. B. and CHEN, C. C. Splashing impact of a single drop onto very thin liquid films. *Physics of Fluids*, **12**(9), 2155–2158 (2000)

[10] COSSALI, G., MARENGO, M., COGHE, A., and ZHDANOV, S. The role of time in single drop splash on thin film. *Experiments in Fluids*, **36**(6), 888–900 (2004)

[11] ELLIS, A., SMITH, F., and WHITE, A. Droplet impact on to a rough surface. *The Quarterly Journal of Mechanics & Applied Mathematics*, **64**(2), 107–139 (2011)

[12] HUNG, Y. L., WANG, M. J., LIAO, Y. C., and LIN, S. Y. Initial wetting velocity of droplet impact and spreading: water on glass and parafilm. *Colloids and Surfaces A: Physicochemical and Engineering Aspects*, **384**(1-3), 172–179 (2011)

[13] VANDER WAL, R. L., BERGER, G. M., and MOZES, S. D. The combined influence of a rough surface and thin fluid film upon the splashing threshold and splash dynamics of a droplet impacting onto them. *Experiments in Fluids*, **40**(1), 23–32 (2006)

[14] BARTHLOTT, W. and NEINHUIS, C. Purity of the sacred lotus, or escape from contamination in biological surfaces. *Planta*, **202**(1), 1–8 (1997)

[15] FENG, L., LI, S., LI, Y., LI, H., ZHANG, L., ZHAI, J., SONG, Y., LIU, B., JIANG, L., and ZHU, D. Super-hydrophobic surfaces: from natural to artificial. *Advanced Materials*, **14**(24), 1857–1860 (2002)

[16] YARIN, A. L. Drop impact dynamics: splashing, spreading, receding, bouncing. *Annual Review Fluid Mechanics*, **38**, 159–192 (2006)

[17] JOSSERAND, C. and THORODDSEN, S. T. Drop impact on a solid surface. *Annual Review of Fluid Mechanics*, **48**, 365–391 (2016)

[18] LEE, M., CHANG, Y. S., and KIM, H. Y. Drop impact on microwetting patterned surfaces. *Physics of Fluids*, **22**(7), 072101 (2010)

[19] KANNAN, R. and SIVAKUMAR, D. Drop impact process on a hydrophobic grooved surface. *Colloids and Surfaces A*: *Physicochemical and Engineering Aspects*, **317**(1-3), 694–704 (2008)

[20] LATKA, A., STRANDBURG-PESHKIN, A., DRISCOLL, M. M., STEVENS, C. S., and NAGEL, S. R. Creation of prompt and thin-sheet splashing by varying surface roughness or increasing air pressure. *Physical Review Letters*, **109**(5), 054501 (2012)

[21] XU, L. Liquid drop splashing on smooth, rough, and textured surfaces. *Physical Review E*, **75**(5), 056316 (2007)

[22] RIOBOO, R., BAUTHIER, C., CONTI, J., VOUE, M., and DE CONINCK, J. Experimental investigation of splash and crown formation during single drop impact on wetted surfaces. *Experiments in Fluids*, **35**(6), 648–652 (2003)

[23] WEISS, D. A. and YARIN, A. L. Single drop impact onto liquid films: neck distortion, jetting, tiny bubble entrainment, and crown formation. *Journal of Fluid Mechanics*, **385**, 229–254 (1999)

[24] JOSSERAND, C. and ZALESKI, S. Droplet splashing on a thin liquid film. *Physics of Fluids*, **15**(6), 1650–1657 (2003)

[25] GUEYFFIER, D. and ZALESKI, S. Finger formation during droplet impact on a liquid film. *Comptes Rendus de l'Académie des Sciences-Series IIB-Mechanics Physics Astronomy*, **12**(326), 839–844 (1998)

[26] COSSALI, G. E., COGHE, A., and MARENGO, M. The impact of a single drop on a wetted solid surface. *Experiments in Fluids*, **22**(6), 463–472 (1997)

[27] LEE, S. H., HUR, N., and KANG, S. A numerical analysis of drop impact on liquid film by using a level set method. *Journal of Mechanical Science and Technology*, **25**(10), 2567 (2011)

[28] MUKHERJEE, S. and ABRAHAM, J. Crown behavior in drop impact on wet walls. *Physics of Fluids*, **19**(5), 052103 (2007)

[29] BRACKBILL, J. U., KOTHE, D. B., and ZEMACH, C. A continuum method for modeling surface tension. *Journal of Computational Physics*, **100**(2), 335–354 (1992)

[30] WELLER, H. G. A new approach to VoF-based interface capturing methods for incompressible and compressible flow. *Technical Report*, OpenCFD Ltd., TR/HGW/04, 35 (2008)

[31] SHETABIVASH, H., OMMI, F., and HEIDARINEJAD, G. Numerical analysis of droplet impact onto liquid film. *Physics of Fluids*, **26**(1), 012102 (2014)